

## Article

# One-Step Process for the Fabrication of Hydrophobic and Dimensional Stable Wood Using Functionalized Silica Nanoparticles

Miklós Bak <sup>1,\*</sup>, Dávid Takács <sup>1</sup>, Rita Rákosa <sup>2</sup>, Zsolt István Németh <sup>2</sup> and Róbert Németh <sup>1</sup><sup>1</sup> Faculty of Wood Engineering and Creative Industries, University of Sopron, H9400 Sopron, Hungary<sup>2</sup> Spectrometry Laboratory, Ingvesting Team Ltd., H9400 Sopron, Hungary

\* Correspondence: bak.miklos@uni-sopron.hu

**Abstract:** The aim of this research was to improve the dimensional stability of wood through bulk hydrophobization, as a result of impregnation with fluorinated silica nanoparticles. The wood species European beech (*Fagus sylvatica* L.) and Scots pine (*Pinus sylvestris* L.) were used. The characterization of the modified wood was performed using analytical methods, including scanning electron microscopy, energy dispersive X-ray spectroscopy, and Fourier-transform infrared spectroscopy. The effect of fluorinated silica nanoparticles on the anti-swelling efficiency, water uptake, equilibrium moisture content, and water contact angle were investigated. The surface of the cell walls was discontinuously covered with fluorinated silica nanoparticles forming a rough surface coating. The presence of the hydrophobic silica nanoparticles improved the dimensional stability by permanently increasing the hydrophobicity of wood, besides a low weight percent gain. Furthermore, the treatment significantly decreased the equilibrium moisture content and water uptake. The modified wood surfaces showed significantly higher water contact angles, which was the main reason of the improved dimensional stability.

**Keywords:** wood modification; hydrophobicity; fluorinated silica nanoparticles; anti-swelling-efficiency; swelling anisotropy; water uptake; contact angle



**Citation:** Bak, M.; Takács, D.; Rákosa, R.; Németh, Z.I.; Németh, R.

One-Step Process for the Fabrication of Hydrophobic and Dimensional Stable Wood Using Functionalized Silica Nanoparticles. *Forests* **2023**, *14*, 651. <https://doi.org/10.3390/f14030651>

Academic Editor: Antonios Papadopoulos

Received: 24 February 2023

Revised: 19 March 2023

Accepted: 20 March 2023

Published: 22 March 2023



**Copyright:** © 2023 by the authors. Licensee MDPI, Basel, Switzerland. This article is an open access article distributed under the terms and conditions of the Creative Commons Attribution (CC BY) license (<https://creativecommons.org/licenses/by/4.0/>).

## 1. Introduction

The importance of wood among renewable raw materials is indisputable, as it is CO<sub>2</sub>-neutral and recyclable. Due to its versatility, it has been used in a wide variety of ways for thousands of years. Thanks to all of this, the demand for wood is constantly increasing. The forest-based sector is aware of these needs and the resulting problems, to which they respond with extensive research and development activities. In general, wood modification is the application of physical, chemical, or biological methods to wood in order to change its properties [1]. In recent decades, the demand for modified wood materials has increased, which has been followed by the increasing commercialization of modification procedures. Utilization of wood is continuously facing new challenges. The aim is to improve the properties of wood (decay and weathering resistance, dimensional stability), resulting in better performance and wider utilization. Extensive research is underway to improve the characteristics of wood. One basic common finding is that moisture absorption is required to be reduced to increase dimensional stability and improve durability [2–4].

The fabrication of hydrophobic surfaces is a promising novel method used to minimize the water adsorption of wood. Fabrication of low-surface-energy surfaces is possible via one-step methods, such as electrospinning, or plasma, laser, or chemical etching [5–7]. Hydrophobic surfaces can also be produced by two-step processes, where a rough layer is first formed on the surface and then modified to become hydrophobic [8–10]. There are also several options for making wooden surfaces hydrophobic. These include chemical modification with acetylation, impregnation by hydrophobic agents (oils, waxes), the

use of metal salts, sol-gel processes, grafting of silicone polymers onto the wood surface, introducing microemulsions into the wood, and layer-by-layer deposition [11,12].

SiO<sub>2</sub> nanoparticles are inexpensive and non-toxic, so they are often used to create nanoscale surface roughness. The strong hydrophobic character is formed during the modification or functionalization of the nanoparticles [5,13–17]. The development of superhydrophobic surfaces has become important in many fields due to the increasing demand for minimal water and/or oil adhesion or self-cleaning surfaces [18–21]. Wood modification methods based on depositing silica nanoparticles on the cell walls have also been studied in recent years, focusing mainly on the hydrophobization or self-cleaning properties of surfaces [6,7,22,23].

An effective solution is the use of fluorinated nanoparticles to create hydrophobic materials [24–27]. However, several methods have already been developed for wood material. These methods primarily focus only on the surface properties of the materials, and only a small amount of information is available on their effects on the wood–water relationships of the bulk wood [15,24,28].

The purpose of this study was to develop a one-step method using fluorinated silica nanoparticles (FSNPs) for the hydrophobization of the cellular structure of wood to improve dimensional stability and to reduce water adsorption capacity. Silica nanoparticles are modified by a fluoroalkyl silane (1H,1H,2H,2H-perfluorodecyltriethoxysilane, FAS-17). The expectation of this research was to improve the dimensional stability by using fluorinated silica nanoparticles during the bulk modification of wood. Traditional sol-gel methods for silica treatment of wood are only effective when using high weight-percent-gains (WPGs) [29]; thus, an additional aim of this research was to remarkably improve dimensional stability of wood using a low WPG treatment.

## 2. Materials and Methods

### 2.1. Materials

Samples of Scots pine sapwood (*Pinus sylvestris* L.) and European beech (*Fagus sylvatica* L.) originating from southwestern Hungary were used with an initial moisture content of  $12 \pm 2\%$ . The density of beech and Scots pine was 658 and 514 kg/m<sup>3</sup>, respectively. Silica nano powder (15 nm, 99.5%) and 1H,1H,2H,2H-perfluorodecyltriethoxysilane (FAS-17, 97%) were obtained from Sigma-Aldrich Co., LLC (Budapest, Hungary); ethanol (ET, 99.99%) was purchased from Merck KGaA (Budapest, Hungary); and distilled water was prepared in the laboratory. All chemicals were used as received without further purification.

### 2.2. Preparation of FSNP Suspension

As a first step, silica nanoparticles were functionalized in the ethanol solution of FAS-17. First, 1 g of silica nanopowder was mixed in 100 mL of ethanol using a magnetic stirrer (Witeg MS2DHS) for 120 min at 50 °C at 1000 rpm. A quantity of 0.5 or 1 g of FAS-17 was further added to this solution to obtain different levels of fluorination while maintaining the stirring. Different suspensions are indicated hereafter as FSNP0.5 and FSNP1.0, respectively. During this step, long perfluoro chains were grafted onto the surface of the silica nanoparticles, so that their originally hydrophilic character became hydrophobic.

### 2.3. Preparation of FSNP-Treated Wood Samples

The test specimens were vacuum impregnated in their final dimensions used in the tests later. Before the impregnation process, the samples were oven dried for 24 h in a drying chamber (Memmert UP 500) at 105 °C. It was followed by a 1 h long vacuum phase at 20 °C using 0.01 MPa pressure in a vacuum dryer (Memmert VO 400). The next step was a 2 h long impregnation under atmospheric pressure while keeping the samples in the suspension. Finally, a two-stage drying phase was used, including drying at 60 °C for 24 h, and at 105 °C for 24 h.

## 2.4. Test Methods

### 2.4.1. Weight Percent Gain (WPG)

To determine WPG (FSNP uptake of the samples), dry weight (before impregnation) and impregnated dry weight (after impregnation) were measured. WPG was calculated according to Equation (1):

$$\text{WPG} = \frac{m_{0,imp} - m_0}{m_0} \cdot 100 [\%] \quad (1)$$

where  $m_{0,imp}$  is the oven-dry weight of samples after impregnation (g) and  $m_0$  is the oven-dry weight of samples before impregnation with FSNP suspension (g). Additionally, retention of treating solids (RET) in  $\text{kg}/\text{m}^3$  was also calculated, showing the specific quantity of the FSNPs deposited in wood.

### 2.4.2. SEM/EDX Analysis

Modified samples were characterized with a Hitachi S-3400N type scanning electron microscope (SEM). Longitudinal (radial or tangential) sections were cut with a razor blade before imaging. All surfaces of the cut SEM samples were at least 5 mm from the initial sample surface. The samples with dimensions of  $5 \times 5$  mm were coated with a gold/palladium layer using a sputter-coater before imaging. An accelerating voltage of 10 kV and a working distance of 5 mm were used during SEM imaging. A Bruker XFlash Detector 5010 type detector was used for energy dispersive X-ray spectrometry (EDX) to analyze the elemental composition. The samples for EDX analysis were used without sputter-coating, to avoid the effect of the gold/palladium coating on the elemental composition. The spatial resolution of Si and F element mapping was  $0.2 \mu\text{m}$ , on a measurement area of  $20 \times 25 \mu\text{m}$ .

### 2.4.3. FT-IR Analysis

FT-IR measurements were performed using a Shimadzu IRAffinity-1 spectrometer equipped with an HATR 10 total reflection accessory kit (Shimadzu Europa GmbH, Duisburg, Germany). The wavenumber range of the spectra was  $4000\text{--}670 \text{ cm}^{-1}$  with a spectral resolution of  $1 \text{ cm}^{-1}$ . The registered spectra were derived as the means of 49 scans each.

Various pre-processing methods were used to eliminate spectral variability. The influence of  $\text{CO}_2$  and air humidity was reduced by atmospheric correction using Shimadzu IRsolution software (Version 1.60, Duisburg, Germany). Additionally, the resolution of the spectrum was smoothed to  $10 \text{ cm}^{-1}$  to reduce the noise amplitude. The relevant deviations in the intensities in the primary spectra are due to the stochastic fitting of wood samples to the ATR crystal and surface roughness, and inhomogeneity. These deviations were eliminated by application of SNV (standard normal variate) transformation as a normalization method. Finally, component analysis (PCA) was used to assess the spectra. PCA decompositions were carried out using the Chemometrics Add-In extension in Microsoft Excel.

### 2.4.4. Water Repellency

An optical goniometer (PocketGoniometer PGX+, Model 68-76, Messmer Büchel, Molenbaan, The Netherlands) was used to determine the contact angle (CA) of deionized water (surface tension:  $3.2 \text{ mN}/\text{m}$ ). The volume of the droplet was set at  $4 \mu\text{L}$ . CA was first measured at 120 ms, followed by measurements at 5, 10, 20, 30, 60, 120, 240, 360, 480 and 570 s. CA was measured at 10 points on each of the 10 samples.

### 2.4.5. Anti-Swelling-Efficiency and Swelling Anisotropy

Anti-swelling-efficiency (ASE) was tested on 20 pieces of  $20 \times 20 \times 30 \text{ mm}^3$  (radial  $\times$  tangential  $\times$  longitudinal) samples of each treated and control material. The samples' dimensions were measured under oven-dry ( $105 \text{ }^\circ\text{C}$ ) and water saturated conditions. The

full saturation was taken as a constant weight of the samples. ASE in radial and tangential directions was calculated according to Equation (2):

$$ASE_{r,t} = \frac{S_{U,r,t} - S_{T,r,t}}{S_{U,r,t}} \cdot 100 [\%] \quad (2)$$

where  $S_{U,r,t}$  is the swelling of control samples in the radial or tangential direction (%), and  $S_{T,r,t}$  is the swelling of treated samples in the radial or tangential direction (%).

Swelling anisotropy was calculated according to Equation (3):

$$A_{sw} = \frac{S_t}{S_r} \quad (3)$$

where  $S_t$  is swelling in tangential direction and  $S_r$  is swelling in the radial direction.

#### 2.4.6. Equilibrium Moisture Content (EMC)

EMC was tested on 10 pieces of  $20 \times 20 \times 5 \text{ mm}^3$  (radial  $\times$  tangential  $\times$  longitudinal) samples of each treated and control material. The samples' weight was measured under oven-dry ( $105 \text{ }^\circ\text{C}$ ) and climatized ( $t = 20 \text{ }^\circ\text{C}$ ;  $\varphi = 65\%$ ) conditions. The constant mass was reached in 10 weeks by all test specimens.

#### 2.4.7. Water Uptake (W)

Water uptake in radial and tangential surfaces was determined separately, using samples with clear radial or tangential surfaces. The sample dimensions were  $10 \times 50 \times 50 \text{ mm}^3$  (radial/tangential  $\times$  tangential/radial  $\times$  longitudinal). Ten pieces for all treatment variations and control were used. The modified and control samples were climatized ( $t = 20 \text{ }^\circ\text{C}$ ;  $\varphi = 65\%$ ). A commercial silicone sealant (Soudal neutral silicone) was applied to the edges and one radial or tangential surface and weighed. Samples were then immersed in distilled water with the unsealed surface for 72 h and weighed. Water uptake was calculated according to Equation (4):

$$W = \frac{m_u - m_0}{A} \left[ \frac{\text{g}}{\text{m}^2} \right] \quad (4)$$

where  $m_u$  is the weight of the samples after water uptake (g),  $m_0$  is the weight of the samples before water uptake (g), and  $A$  is the immersed surface area of the samples ( $\text{mm}^2$ ).

#### 2.4.8. Statistical Analysis of the Results

The distribution normality of the data was verified and statistical significance tests (ANOVA, Fischer LSD-test,  $p < 0.05$ ) were conducted for the effect of the treatment on the investigated material properties with the software Statistica (Statsoft, Version 13.0, Palo Alto, CA, USA).

### 3. Results and Discussion

#### 3.1. WPG

Wood species did not have a significant effect on WPG (Table 1), but beech samples' variation coefficients were significantly lower, which indicates a more uniform penetration of the FSNPs in beech wood measured by quantity. However, this does not yet imply a uniform distribution of FSNPs in the wood structure. The WPG (the ratio of FSNPs deposited in wood) was an average of 0.74%–1.16%, depending on treatment type (FSNP0.5 or FSNP1.0) and wood species. This WPG is explicitly low, in comparison to most of the silica-based modification methods, which usually show WPG in the range of 20%–60% [29]. However, there was a significant difference between the retention of beech and pine. It was approximately 55% higher for beech in all treatments, indicating a higher level of impregnation compared to pine. Impregnability of beech and Scots pine sapwood is similar [30], but the different anatomical structure and porosity results in different retention.

**Table 1.** WPG and RET values of FSNP-modified beech and Scots pine samples.

	Beech				Pine			
	FSNP0.5		FSNP1.0		FSNP0.5		FSNP1.0	
	WPG [%]	RET [kg/m <sup>3</sup> ]						
Mean	0.78	6.15	1.16	8.84	0.74	3.87	1.10	5.66
Min	0.70	0.29	1.00	0.67	0.59	0.46	0.84	0.70
Max	0.88	5.71	1.25	7.27	0.95	3.21	1.36	4.62
St. Dev.	0.06	6.61	0.07	9.60	0.10	4.86	0.17	6.67
Var. Coeff.	7.26%	4.76%	5.83%	7.59%	13.87%	11.94%	15.77%	12.34%

### 3.2. SEM Imaging

SEM imaging was undertaken for both wood species, but the distribution and morphology of the nanoparticles was not affected by the wood species. Therefore, only SEM micrographs of Scots pine are shown in Figure 1. FSNPs do not completely cover the cell wall surface and are visible as small, rough depositions (Figure 1a,b). Additionally, the FSNPs showed some agglomerations and larger deposits in the cell lumens (Figure 1c). Although these FSNP agglomerations do not clog the lumens completely, they improve the dimensional stabilization effect of this modification method [31]. FSNP coating is non-continuous on the cell wall surfaces, but it provides secondary surface roughness at micro- and nano-levels to them, which is known to result in higher hydrophobicity [32]. The uniform distribution and effective size of nanoparticles may contribute to reduced hygroscopicity, which leads to increased dimensional stability [33–35].

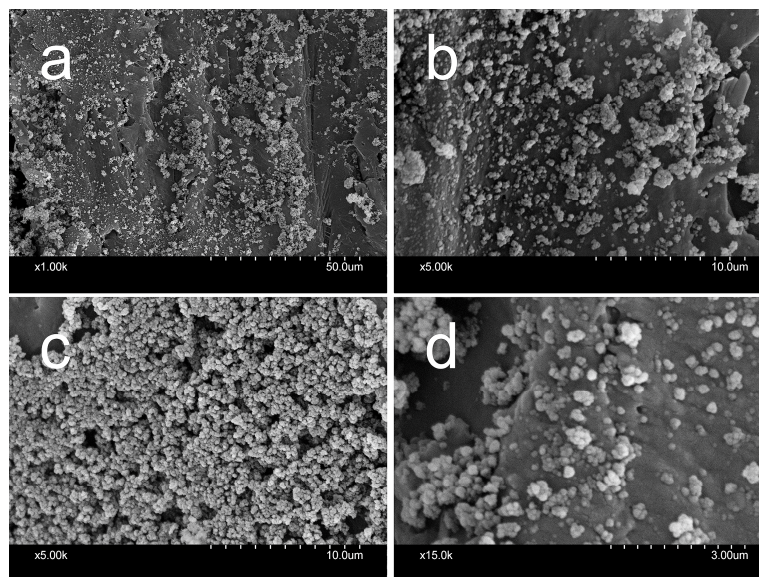


**Figure 1.** SEM images of the FSNP1.0-modified Scots pine wood in tangential section. (a,b,d): FSNPs deposited on cell wall surface, (c) the loose/porous structure of FSNP deposits on the cell wall surface.

The discontinuous FSNP layer on the cell wall surfaces is the result of the low concentration of the FSNPs in the modifying suspension (1.5 and 2 wt.%). This meets the objective of keeping the amount of FSNPs in the wood low. The loose/porous structure of FSNP deposits is clearly shown in Figure 1c,d. Although the determination of the diameters of FSNP spheres is difficult, because they overlap in the image, a rough estimation of the globule size is 50 to 200 nm.

### 3.3. EDX Analysis

The elemental analysis of the samples revealed the position and distribution of FSNPs in the wood. This method supported the data from SEM imaging, as in general, an even distribution of the particles was found, besides some smaller agglomerations (Figure 2). Quantitative analysis indicated 3.43 wt.% silicon and 0.19 wt.% fluorine on pine wood (Table 2). This means that FSNPs are deposited in the wood, as the wood itself does not contain the Si element at such high levels. This result shows that FSNP suspension can easily be brought into the structure of both beech and pine wood, as the samples for this test were obtained from the middle the modified wood.

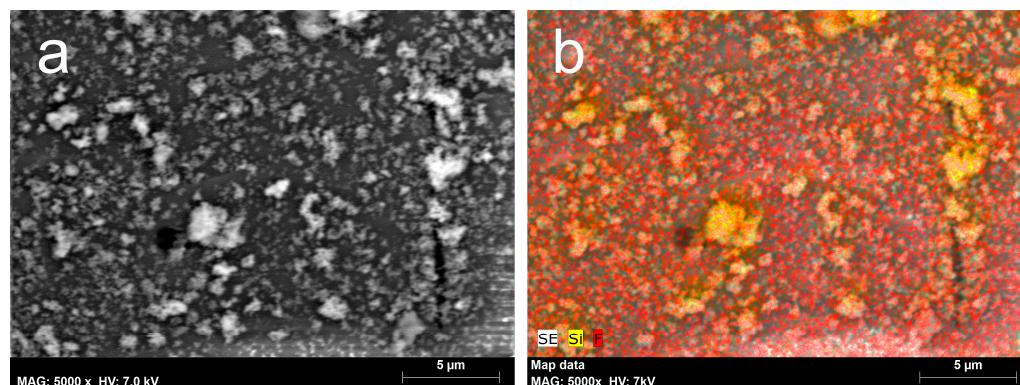


**Figure 2.** EDX map of FSNP-treated (FSNP1.0) pine wood in tangential section. (a) SE image of an FSNP-treated earlywood tracheid cell wall surface. (b) Distribution of Si and F elements on the same surface, combined with SE image. Red color indicates presence of fluorine, yellow color indicates presence of silica.

**Table 2.** Quantitative elemental composition of the FSNP-treated (FSNP1.0) Scots pine earlywood tracheid cell wall surface shown in Figure 2.

Element	[wt.%]	[at.%]	Error in wt.%
Carbon	63.99	71.18	6.58
Oxygen	32.39	27.05	3.41
Fluorine	0.19	0.13	0.05
Silicon	3.43	1.63	0.16
Sum:	100	100	

### 3.4. FT-IR Analysis

Wood has a complicated chemical structure and contains several light-absorbing functional groups and moieties. The characteristic absorption peaks are derived from the chemical components of the wood: cellulose, lignin, and hemicellulose. The spectra were evaluated only in the fingerprint region, where absorption bands characteristic of the samples are found. Assignment of absorption bands was performed based on the literature [36–39].

Chemical changes in the wood surface as a result of FSNP modification can be detected by the FT-IR spectra. Small differences are visible between the transformed SNV spectra of beech and Scots pine due to differences in their chemical composition (Figure 3). The broad band in the spectra of FSNP-modified wood observed in the range 850–1300  $\text{cm}^{-1}$  was attributed to the overlapped stretching vibrations of Si–O–Si, C–F, and C–O–C bonds [40]. On the left side of this band, two small shoulders between 1130 and 1250  $\text{cm}^{-1}$  were assigned to the stretching vibration of C–F bonds [41,42]. The absorption peaks at 1079 and 789  $\text{cm}^{-1}$  correspond to the asymmetric stretching vibration and bending mode of Si–O–Si bonds in the silica nanoparticles [14,37,38,43]. The presence of C–F and Si–O–Si bonds proves the successful impregnation with fluorinated silica nanoparticles.

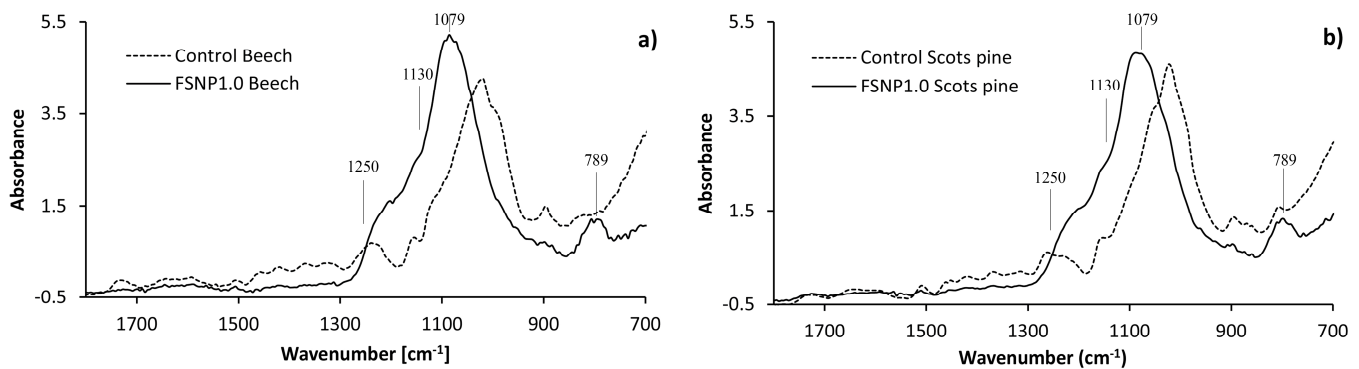


**Figure 3.** SNV-transformed FT-IR spectra of control and FSNP1.0-modified wood: (a) beech, (b) Scots pine.

The hidden information in the complex light absorption peaks of ATR-FTIR spectra can be revealed by a multivariate data evaluation method [44]. PCA can visualize the latent information in the spectra by projecting them into a multidimensional space of the principal components (PCs). Each dimension in the PC's space corresponds to the linear combinations of the different variables as wavenumbers in the spectrum. The absorbance values on the coordinate axes determine the distances from the origin. The PCA decomposition of the spectra showed the differences between the wood species and the effect of the modifications (Figure 4). The PC1 axis represents the treatment and the PC2 axis represents the wood species, while distances from the centroids give information on the extent of molecular changes. In the case of modified Scots pine, the samples are shown to separate into two groups along the PC1 axis, representing the different level of NP fluorination. For the modified beech results, similar group separation is not reflected by PCA resolution. This indicates higher variation in the chemical changes as a result of the modification in beech.

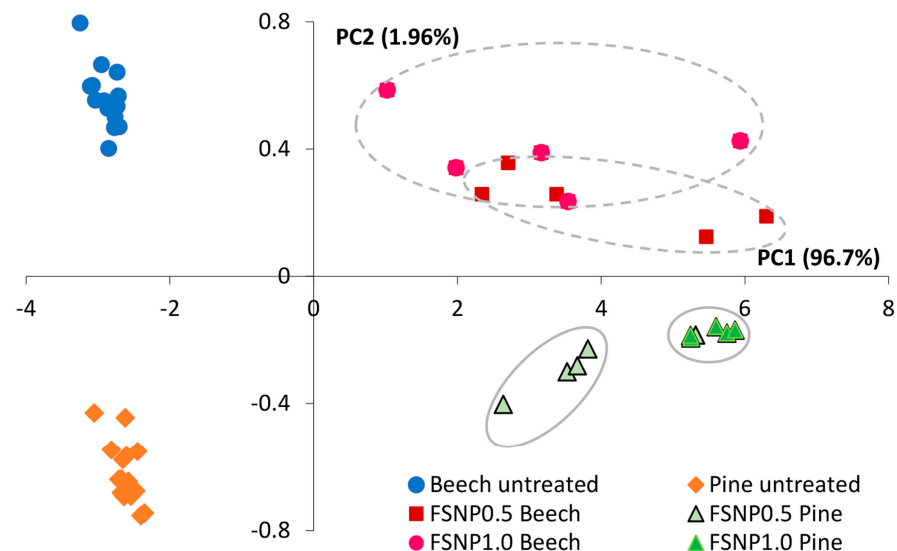


**Figure 4.** PCA score plot of the untreated and FSNP1.0-modified wood in the 1800–800  $\text{cm}^{-1}$  spectral region.

### 3.5. Water Repellency

FSNP treatment resulted in a high hydrophobization effect (Figure 5). The initial CA (at time = 120 ms) of the untreated samples was found to be 67.3–69.3° without showing a significant difference between wood species. CAs increased significantly on the FSNP-treated wood surfaces (132.4–147.8°), depending on the treatment type. A higher

proportion of hydrophobic modifier resulted in improved water repellency, as the addition of 1% FAS17 significantly increased the CA, by an additional 15° on average. No difference in the CA could be detected between wood species. The observed CAs are close to the superhydrophobic region (>150°). The effect of FSNP treatments is long-lasting, regardless of the degree of fluorination, as the CA decreases only slowly. Water droplets persisted for a longer time on the surface of FSNP-modified wood, in contrast to the immediate penetration of water into untreated wood.

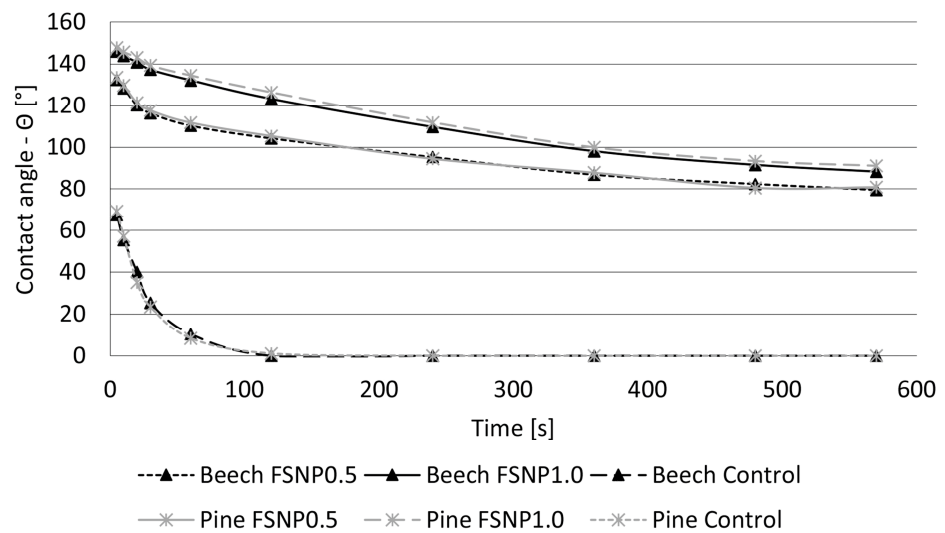


**Figure 5.** Contact angles as a function of time on control and FSNP-modified beech and Scots pine wood surfaces.

3.6. Anti-Swelling-Efficiency (ASE) and Swelling Anisotropy

FSNP treatments decreased swelling remarkably in both wood species. FSNP-modified beech showed significantly lower ASE compared to Scots pine (Figure 6). As expected, the different anatomical structure of the wood species affected the efficiency of the treatments. The higher fluorination level of SNPs resulted in only slightly higher ASE values. Although it was a significant difference, it was not remarkable. Thus, further increasing the fluorination level of SNPs does not appear to be beneficial. The slight differences in WPG (Table 1) did not affect the ASE, as no correlation was found between these two properties.

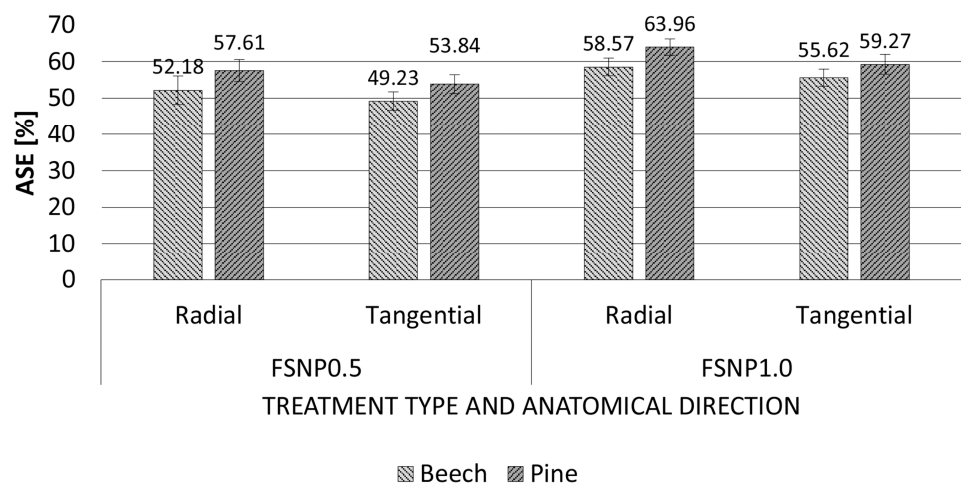


**Figure 6.** ASE of FSNP-modified beech and Scots pine wood in radial and tangential directions (whiskers show standard deviation of the results).

FSNPs partly covered the cell wall surface, which also contributes to the lower swelling through delaying the diffusion of water into the wooden cell wall. The improved ASE is also in line with the improved hydrophobicity of the FSNP-treated wood. The permanent hydrophobizing effect of the treatments largely explains the improvement in the dimensional stability of wood. The effect of nano-SiO<sub>2</sub> to improve water repellency is already known for fiber-reinforced composites based on lignocellulosic waste material and nano-SiO<sub>2</sub> [45]. The superhydrophobic effect of the perfluoroalkyl methacrylic co-polymer and silica nanosphere based fluoro-containing silica nanocoating was also demonstrated on wooden surfaces [24].

Despite the low levels of FSNPs in wood (Table 1), ASE was high, ranging from 49.23% to 63.96%, depending on treatment type and wood species. Besides the improved hydrophobic character, this was attributed to the clogging effect of the nanoparticles by occupying void spaces in the wood tissue [46–49]. Overall, this results in the FSNP layers on the cell wall surfaces blocking water molecules from the bonding sites.

Higher ASE values were found in the radial direction, compared to the tangential direction; however, it did not increase the swelling anisotropy statistically significantly (Figure 7). Thus, the treatment is not expected to lead to the increased likelihood of cracks, deformations, and warping during utilization under changing climatic conditions.

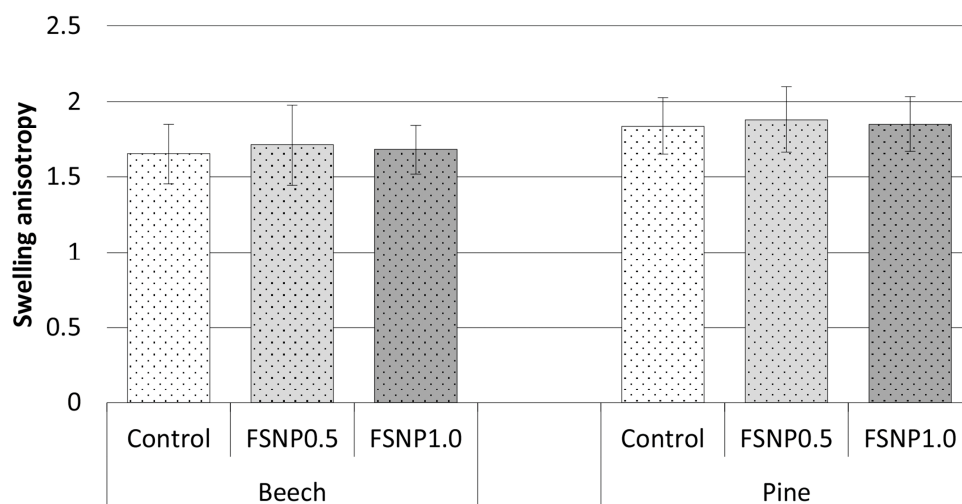


**Figure 7.** Swelling anisotropy of FSNP-modified beech and Scots pine wood (whiskers showing standard deviation of the results).

### 3.7. Equilibrium Moisture Content

FSNP treatment significantly decreased EMC by 6%–16%, which is, however, not a remarkable change (Figure 8). This means that besides producing a highly water-resistant surface, the moisture-absorbing ability of wood was also decreased. The slight decrease in moisture uptake as a result of FSNP deposition in wood tissue is explained by the combined effect of the nanoparticles, including clogging the void spaces and being hydrophobic [49]. Sufficiently small-sized nanoparticles can penetrate the cell wall pores, inhibiting moisture from entering and, in this way, decreasing water absorption [50,51]. Similarly, FSNPs may also block sorption sites of wood cell lumens and those directly in the cell walls [52]. This effect is described as the obstruction of micro-capillaries in wood by the particles, so that water loses its main channel for penetration into the cell wall. In addition, many hydrophilic functional groups on wooden cell walls may be replaced by some functional group of SiO<sub>2</sub> nanoparticles, and the bound water that is located within the cell wall can be replaced by them [50,53]. The relatively low decrease in the EMC can be attributed to the discontinuous FSNP layer on the cell wall surfaces (Figure 1), thus explaining the contact of the cell wall surfaces, and water vapor was not completely blocked physically. Scots pines EMC showed a remarkably higher decrease, despite the higher WPG values for beech.

However, a higher amount of FAS17 used for the fluorination of SNPs resulted in, only in the case of pine wood, a slightly but significantly lower EMC.

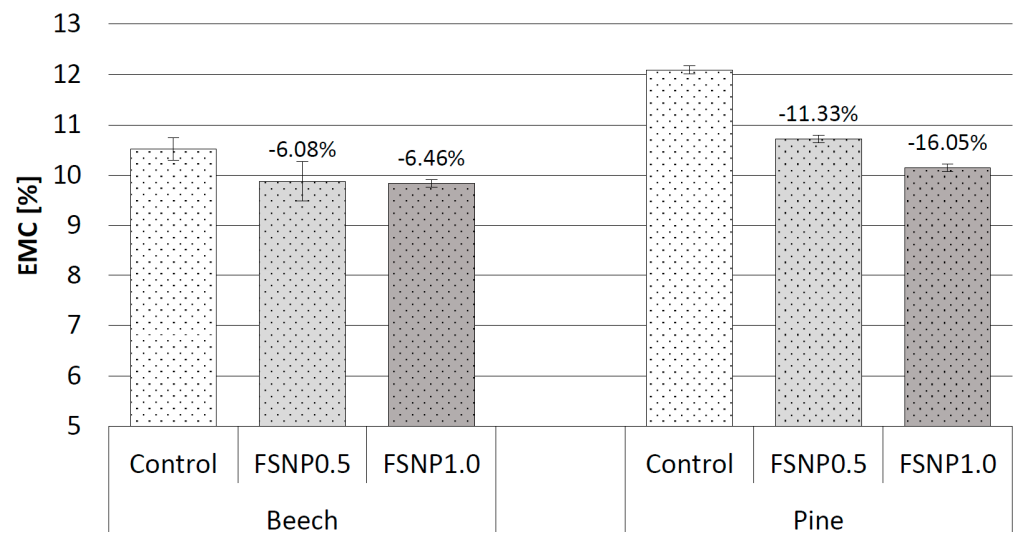


**Figure 8.** Equilibrium moisture content of FSNP-treated beech and Scots pine wood (percentages show the difference to the control and whiskers the standard deviation of the results).

### 3.8. Water Uptake

The presence of FSNPs in the wood resulted in significantly lower water uptake (Figure 9). These results indicated that the amount of FSNPs and their fixation to the cell wall surfaces was enough to exclude water from cell lumens [23]. In addition, FSNPs increasingly block cell wall pits and micropores, which further enhances the barrier effect of FSNPs, which fill the voids and inhibit water absorption more effectively [32]. The FSNPs and their depositions created a nano-structured layer on the cell wall surfaces (Figure 1) with increased roughness, resulting in reduced surface free energy and lower capillarity of the cell lumens. This nano-scale surface roughness mimics the “lotus effect” known from nature [32,54]. Additionally, the longer and more tortuous path provided by the deposited FSNP layers further impedes water transport [34,46].

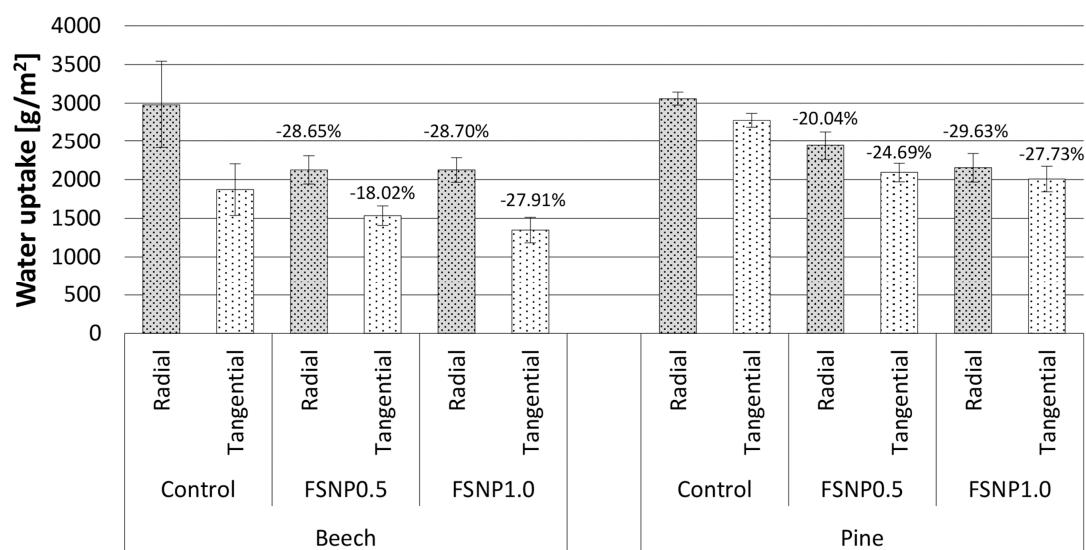


**Figure 9.** Water uptake of FSNP-treated and untreated beech and Scots pine wood in radial and tangential directions (percentages show the difference to the control and whiskers the standard deviation of the results).

The absorption of water vapor (EMC) decreased much less than the water uptake. Water uptake showed a decrease of 18.02%–29.63%, while EMC decreased by only 6.08%–18.05%, depending on the parameters. The hydrophobization effect of the FSNPs explains the difference between water uptake and water vapor sorption. A higher amount of FAS17 used for the fluorination of SNPs did not result in significantly lower water uptake.

#### 4. Conclusions

It was proved that the impregnation of wood by fluorinated silica nanoparticles remarkably improves dimensional stability. Anatomical direction did not affect the ASE (49.23%–63.96%); however, wood species had a slight, but statistically significant, effect on it. Swelling anisotropy was not changed. Hydrophobic fluorinated silica nanoparticles were deposited on the cell wall surfaces, thus making the wood water repellent. However, the liquid water uptake was significantly inhibited, showing 18.02%–28.70% lower values, whereas water vapor sorption was only inhibited through the fluorinated silica nanoparticles by a lower ratio (−6.08%–11.33%). SEM imaging and EDX mapping showed that the hydrophobic fluorinated silica nanoparticles did not continuously cover the cell wall surfaces and some small, rough depositions were also present. The result of the non-continuous covering of the cell wall surfaces was a smaller decrease in the equilibrium moisture uptake. The positive effect of the treatment can be explained by a combination of different phenomena. Nanoparticles form a coating on the cell wall surface, which acts as a hydrophobic barrier on the surface, with low surface energy. Additionally, they penetrate the micropores and cause a clogging effect.

**Author Contributions:** Conceptualization, M.B.; methodology, M.B.; validation, R.N.; formal analysis, M.B.; investigation, M.B., D.T., R.R. and Z.I.N.; resources, M.B. and R.N.; data curation, M.B., R.R. and R.N.; writing—original draft preparation, M.B., R.R., Z.I.N. and R.N.; visualization, M.B. and R.R.; supervision, M.B. and R.N.; project administration, M.B.; funding acquisition, M.B. All authors have read and agreed to the published version of the manuscript.

**Funding:** Project no. FK 142527 has been implemented with the support provided by the Ministry of Innovation and Technology of Hungary from the National Research, Development and Innovation Fund, financed under the “FK22 OTKA” funding scheme.

**Data Availability Statement:** Not applicable.

**Conflicts of Interest:** The authors declare no conflict of interest. The funders had no role in the design of the study; in the collection, analyses, or interpretation of data; in the writing of the manuscript; or in the decision to publish the results.

#### References

1. Hill, C.A.S. *Wood Modification: Chemical, Thermal and Other Processes*, 1st ed.; John Wiley & Sons, Ltd.: Chichester, UK, 2006; pp. 19–21.
2. Mahltig, B.; Swaboda, C.; Roessler, A.; Böttcher, H. Functionalising wood by nanosol application. *J. Mater. Chem.* **2008**, *27*, 3180–3192. [[CrossRef](#)]
3. Rassam, G.; Abdib, Y.; Abdia, A. Deposition of TiO<sub>2</sub> nano-particles on wood surfaces for UV and moisture protection. *J. Exp. Nanosci.* **2012**, *7*, 468–476. [[CrossRef](#)]
4. Sahin, H.T.; Mantanis, G.I. Nano-based surface treatment effects on swelling, water sorption and hardness of wood. *Maderas Cienc. Tecnol.* **2011**, *13*, 41–48. [[CrossRef](#)]
5. Chen, H.; Zhang, Y.; Zhong, T.; Wu, Z.; Zhan, X.; Ye, J. Thermal insulation and hydrophobization of wood impregnated with silica aerogel powder. *J. Wood Sci.* **2020**, *66*, 81. [[CrossRef](#)]
6. Soytürk, E.E.; Kartal, S.N.; Onses, M.S.; Celik, N. Preliminary evaluation of polydimethylsiloxane and hydrophobic silica nanoparticles to improve water repellency and boron leachability in wood. *Eur. J. Wood Wood Prod.* **2023**, *81*, 89–98. [[CrossRef](#)]
7. Xu, E.; Zhang, Y.; Lin, L. Improvement of mechanical, hydrophobicity and thermal properties of Chinese fir wood by impregnation of nano silica sol. *Polymers* **2020**, *12*, 1632. [[CrossRef](#)]
8. Liang, J.; Li, D.; Wang, D.; Liu, K.; Chen, L. Preparation of stable superhydrophobic film on stainless steel substrate by a combined approach using electrodeposition and fluorinated modification. *Appl. Surf. Sci.* **2014**, *293*, 265–270. [[CrossRef](#)]
9. Paul, B.; Martens, W.N.; Frost, R.L. Surface modification of alumina nanofibres for the selective adsorption of alachlor and imazaquin herbicides. *Colloid Interface Sci.* **2011**, *360*, 132–138. [[CrossRef](#)]

10. Saleema, N.; Sarkar, D.; Gallant, D.; Paynter, R.; Chen, X.-G. Chemical nature of superhydrophobic aluminum alloy surfaces produced via a one-step process using fluoroalkyl-silane in a base medium. *ACS Appl. Mater. Interfaces* **2011**, *3*, 4775–4781. [[CrossRef](#)]
11. Wang, C.; Piao, C. From hydrophilicity to hydrophobicity: A critical review—Part II: Hydrophobic conversion. *Wood Fiber Sci.* **2011**, *43*, 41–56.
12. Kryński, K.; Kowaluk, G. Application of beeswax as a hydrophobic agent in MDF technology. *Ann. Wars. Univ. Life Sci. SGGW* **2021**, *114*, 59–69. [[CrossRef](#)]
13. Athauda, T.J.; Decker, D.S.; Ozer, R.R. Effect of surface metrology on the wettability of SiO<sub>2</sub> nanoparticle coating. *Mater. Lett.* **2012**, *67*, 338–341. [[CrossRef](#)]
14. Brassard, J.-D.; Sarkar, D.K.; Perron, J. Fluorine based superhydrophobic coatings. *Appl. Sci.* **2012**, *2*, 453–464. [[CrossRef](#)]
15. Xu, B.; Cai, Z.; Wang, W.; Ge, F. Preparation of superhydrophobic cotton fabrics based on SiO<sub>2</sub> nanoparticles and ZnO nanorod arrays with subsequent hydrophobic modification. *Surf. Coat. Technol.* **2010**, *204*, 1556–1561. [[CrossRef](#)]
16. Xu, L.; He, J. Fabrication of highly transparent superhydrophobic coatings from hollow silica nanoparticles. *Langmuir* **2012**, *28*, 7512–7518. [[CrossRef](#)]
17. Zhou, H.; Wang, H.; Niu, H.; Gestos, A.; Lin, T. Robust, self-healing superamphiphobic fabrics prepared by two-step coating of fluoro-containing polymer, fluoroalkyl silane, and modified silica nanoparticles. *Adv. Funct. Mater.* **2013**, *23*, 1664–1670. [[CrossRef](#)]
18. Chang, K.-C.; Chen, Y.-K.; Chen, H. Fabrication of highly transparent and superhydrophobic silica-based surface by TEOS/PPG hybrid with adjustment of the pH value. *Surf. Coat. Technol.* **2008**, *202*, 3822–3831. [[CrossRef](#)]
19. Guo, M.; Kang, Z.; Li, W.; Zhang, J. A facile approach to fabricate a stable superhydrophobic film with switchable water adhesion on titanium surface. *Surf. Coat. Technol.* **2014**, *239*, 227–232. [[CrossRef](#)]
20. Sarkar, D.; Saleema, N. One-step fabrication process of superhydrophobic green coatings. *Surf. Coat. Technol.* **2010**, *204*, 2483–2486. [[CrossRef](#)]
21. Wang, Y.; Wang, L.; Wang, S.; Wood, R.J.; Xue, Q. From natural lotus leaf to highly hard-flexible diamond-like carbon surface with superhydrophobic and good tribological performance. *Surf. Coat. Technol.* **2012**, *206*, 2258–2264. [[CrossRef](#)]
22. Ebrahimi, F.; Farazi, R.; Karimi, E.Z.; Beygi, H. Dichlorodimethylsilane mediated one-step synthesis of hydrophilic and hydrophobic silica nanoparticles. *Adv. Powder Technol.* **2017**, *28*, 932–937. [[CrossRef](#)]
23. Wang, X.; Chai, Y.; Liu, J. Formation of highly hydrophobic wood surfaces using silica nanoparticles modified with long-chain alkylsilane. *Holzforschung* **2013**, *67*, 667–672. [[CrossRef](#)]
24. Hsieh, C.-T.; Chang, B.-S.; Lin, J.-Y. Improvement of water and oil repellency on wood substrates by using fluorinated silica nanocoating. *Appl. Surf. Sci.* **2011**, *257*, 7997–8002. [[CrossRef](#)]
25. Wang, S.; Liu, C.; Liu, G.; Zhang, M.; Li, J.; Wang, C. Fabrication of superhydrophobic wood surface by a sol-gel process. *Appl. Surf. Sci.* **2011**, *258*, 806–810. [[CrossRef](#)]
26. Cai, Y.; Li, J.; Yi, L.; Yan, X.; Li, J. Fabricating superhydrophobic and oleophobic surface with silica nanoparticles modified by silanes and environment-friendly fluorinated chemicals. *Appl. Surf. Sci.* **2018**, *450*, 102–111. [[CrossRef](#)]
27. Martin, S.; Brown, P.S.; Bhush, B. Fabrication techniques for bioinspired, mechanically-durable, superliquiphobic surfaces for water, oil, and surfactant repellency. *Adv. Colloid Interface Sci.* **2017**, *241*, 1–23. [[CrossRef](#)]
28. Chang, H.; Tu, K.; Wang, X.; Liu, J. Fabrication of mechanically durable superhydrophobic wood surfaces using polydimethylsiloxane and silica nanoparticles. *RSC Adv.* **2015**, *5*, 30647–30653. [[CrossRef](#)]
29. Donath, S.; Miltz, H.; Mai, C. Wood modification with alkoxy silanes. *Wood Sci. Technol.* **2004**, *38*, 555–566. [[CrossRef](#)]
30. EN 350:2016; Durability of wood and wood-based products—Testing and classification of the durability to biological agents of wood and wood-based materials. European Committee for Standardization: Brussels Belgium, 2016.
31. Götze, J.; Möckel, R.; Langhof, N.; Hengst, M.; Klinger, M. Silicification of wood in the laboratory. *Ceram. Silik.* **2008**, *52*, 268–277.
32. Dong, Y.; Yan, Y.; Zhang, S.; Li, J.; Wang, J. Flammability and physical-mechanical properties assessment of wood treated with furfuryl alcohol and nano-SiO<sub>2</sub>. *Eur. J. Wood Wood Prod.* **2015**, *73*, 457–464. [[CrossRef](#)]
33. Clausen, C.A.; Yang, V.W.; Arang, R.A.; Green, F. Feasibility of nanozinc oxide as a wood preservative. *Am. Wood Prot. Assoc. Proceeding* **2009**, *105*, 255–260.
34. Clausen, C.A.; Green, F.; Kartal, S.N. Weatherability and leach resistance of wood impregnated with nano-zinc oxide. *Nanoscale Res. Lett.* **2010**, *5*, 1464–1467. [[CrossRef](#)] [[PubMed](#)]
35. Freeman, M.H.; McIntyre, C.R. Comprehensive review of copper-based wood preservatives. *For. Prod. J.* **2008**, *58*, 21–27.
36. Pandey, K.; Pitman, A. FTIR studies of the changes in wood chemistry following decay by brown-rot and white-rot fungi. *Int. Biodeter. Biodegr.* **2003**, *52*, 151–160. [[CrossRef](#)]
37. Gwon, J.G.; Lee, S.Y.; Doh, G.H.; Kim, J.H. Characterization of chemically modified wood fibers using FTIR spectroscopy for biocomposites. *J. Appl. Polym. Sci.* **2010**, *116*, 3212–3219. [[CrossRef](#)]
38. Yue, D.; Feng, Q.; Huang, X.; Zhang, X.; Chen, H. In situ fabrication of a superhydrophobic ORMOSIL coating on wood by an ammonia-HMDS vapor treatment. *Coatings* **2019**, *9*, 556. [[CrossRef](#)]
39. Báder, M.; Németh, R.; Sandak, J.; Sandak, A. FTIR analysis of chemical changes in wood induced by steaming and longitudinal compression. *Cellulose* **2020**, *27*, 6811–6829. [[CrossRef](#)]

40. Szubert, K.; Dutkiewicz, A.; Dutkiewicz, M.; Maciejewski, H. Wood protective coatings based on fluorocarbonsilane. *Cellulose* **2019**, *26*, 9853–9861. [[CrossRef](#)]
41. Brassard, J.-D.; Sarkar, D.K.; Perron, J. Synthesis of monodisperse fluorinated silica nanoparticles and their superhydrophobic thin films. *ACS Appl. Mater. Interfaces* **2011**, *3*, 3583–3588. [[CrossRef](#)]
42. Startek, K.; Szczurek, A.; Tran, T.N.L.; Krzak, J.; Bachmatiuk, A.; Lukowiak, A. Structural and functional properties of fluorinated silica hybrid barrier layers on flexible polymeric foil. *Coatings* **2021**, *11*, 573. [[CrossRef](#)]
43. Fu, Y.; Liu, X.; Cheng, F.; Sun, J.; Qin, Z. Modification of the wood surface properties of *Tsoongiodendron odorum* Chun with silicon dioxide by a sol-gel method. *BioResources* **2016**, *11*, 10273–10285. [[CrossRef](#)]
44. Chen, H.; Ferrai, C.; Angiuli, M.; Yao, J.; Raspi, C.; Bramanti, E. Qualitative and quantitative analysis of wood samples by Fourier transform infrared spectroscopy and multivariate analysis. *Carbohydr. Polym.* **2010**, *82*, 772–778. [[CrossRef](#)]
45. Hosseini, S.B.; Hedjazi, S.; Jamalirad, L.; Sukhtesaraie, A. Effect of nano-SiO<sub>2</sub> on physical and mechanical properties of fiber reinforced composites (FRCs). *J. Indian Acad. Wood Sci.* **2014**, *11*, 116–121. [[CrossRef](#)]
46. Devi, R.R.; Maji, T.K. Effect of nano-ZnO on thermal, mechanical, UV stability, and other physical properties of wood polymer composites. *Ind. Eng. Chem. Res.* **2012**, *51*, 3870–3880. [[CrossRef](#)]
47. Soltani, M.; Najafi, A.; Yousefian, S.; Naji, H.R.; Suhaimi, B.E. Water repellent effect and dimension stability of beech wood impregnated with nano-zinc oxide. *BioResources* **2013**, *8*, 6280–6287. [[CrossRef](#)]
48. Habibzade, S.; Taghiyari, H.R.; Omidvar, A.; Roudi, H.R. Effects of impregnation with styrene and nano-zinc oxide on fire-retarding, physical, and mechanical properties of poplar wood. *CERNE* **2016**, *22*, 465–474. [[CrossRef](#)]
49. Kumar, A.; Ryparová, P.; Škapin, A.S.; Humar, M.; Pavlič, M.; Tywoniak, J.; Hajek, P.; Žigon, J.; Petrič, M. Influence of surface modification of wood with octadecyltrichlorosilane on its dimensional stability and resistance against *Coniophora puteana* and molds. *Cellulose* **2016**, *23*, 3249–3263. [[CrossRef](#)]
50. Dirna, F.C.; Rahayu, I.; Zaini, L.H.; Darmawan, W.; Prihatini, E. Improvement of fast-growing wood species characteristics by MEG and nano SiO<sub>2</sub> impregnation. *J. Korean Wood Sci. Technol.* **2020**, *48*, 41–49. [[CrossRef](#)]
51. Mantanis, G.; Papadopoulos, N.N. Reducing the thickness swelling of wood based panels by applying a nanotechnology compound. *Eur. J. Wood Wood Prod.* **2010**, *68*, 237–239. [[CrossRef](#)]
52. Cai, X.; Riedl, B.; Zhang, S.Y.; Wan, H. Effects of nanofillers on water resistance and dimensional stability of solid wood modified by melamine-urea-formaldehyde resin. *Wood Fiber Sci.* **2007**, *39*, 307–318.
53. Shi, J.; Zhou, L.I.J.; Zhang, W.D. Improvement of wood properties by urea-formaldehyde resin and nano-SiO<sub>2</sub>. *Front. For. China* **2007**, *2*, 104–109. [[CrossRef](#)]
54. Neinhuis, C.; Barthlott, W. Characterization and distribution of water-repellent, self-cleaning plant surfaces. *Ann. Bot.* **1997**, *79*, 667–677. [[CrossRef](#)]

**Disclaimer/Publisher’s Note:** The statements, opinions and data contained in all publications are solely those of the individual author(s) and contributor(s) and not of MDPI and/or the editor(s). MDPI and/or the editor(s) disclaim responsibility for any injury to people or property resulting from any ideas, methods, instructions or products referred to in the content.